# Selective Plane Illumination Microscopy with a Light Sheet of Uniform Thickness Formed by an Electrically Tunable Lens

PER NIKLAS HEDDE AND ENRICO GRATTON\*

Laboratory for Fluorescence Dynamics, Department of Biomedical Engineering, University of California, Irvine, California, USA

KEY WORDS fluorescence microscopy; light sheet microscopy; fluorescence fluctuation spectroscopy

ABSTRACTLight sheet microscopy is a powerful technique for rapid, three-dimensional fluorescence imaging of large specimen such as drosophila and zebrafish embryos. Yet, beam divergence results in a loss of axial resolution at the periphery of the light sheet. Here, we demonstrate how an electrically tunable lens can be utilized to maintain the minimal, diffraction-limited thickness of the light sheet over a wide field of view (>600 µm) at high frame rates (40 fps). This mode of operation is necessary for the application of fluorescence fluctuation spectroscopy in images. Microsc. Res. Tech. 81:924-928, 2018. © 2016 Wiley Periodicals, Inc.

## INTRODUCTION

With its high spatiotemporal resolution, axial sectioning capability and low light exposure levels, light sheet microscopy is the ideal tool for in vivo fluorescence imaging of biological specimen up to one millimeter in size. In its original conception, a cylindrical lens is used to generate a thin sheet of light that is injected from the side to illuminate the focal plane of the detection lens (Voie et al., 1993; Huisken et al., 2004). Due to this confinement of the illumination, out-of-focus background is minimized. The propagation length over which the minimal thickness is maintained is called the Rayleigh length. It defines the distance,

$$z_R = \frac{\pi \omega_0^2}{\lambda},\tag{1}$$

at which the cross section of a Gaussian beam has doubled. The beam waist at the focal point,  $\omega_0$ , can be approximated by

$$\omega_0 \approx \frac{\lambda}{\pi NA},$$
 (2)

where  $\lambda$  is the light wavelength and NA the numerical aperture of the focusing lens. Consequently, while the axial resolution increases only linearly with increasing NA, the field of view (FOV) with optimal axial resolution decreases with the square of the NA. This relation results in a fundamental design problem, i.e., a large FOV is not compatible with high axial resolution. For example, with 488-nm excitation light, a Rayleigh length of 500  $\mu$ m restricts the sheet thickness to  $\sim$ 9  $\mu$ m (NA 0.02) while a 1 µm thickness (NA 0.3) results in a Rayleigh length of only 6.4 µm. To overcome this limitation, various ways to minimize beam divergence have been proposed. Sample illumination with non-Gaussian beams such as Bessel and Airy beams has lead to substantial improvements in the ratio of axial resolution to FOV (Fahrbach and Rohrbach, 2010; Planchon et al., 2011; Vettenburg et al., 2014). However, those beams

comprise side lobes that illuminate neighboring planes. To avoid image artifacts, either non-linear, multi-photon excitation or structured illumination and/or image deconvolution must be used. Another approach to maintain high axial resolution was derived from confocal slit scanning microscopy, in which the sample is scanned with a light sheet propagating along the optical axis of the detection lens. To suppress out-of-focus fluorescence, this line is reimaged on a slit and can be detected by subsequent scanning across a camera chip. Many modern sCMOS cameras feature a rolling shutter that can be configured as a virtual slit which simplifies the optical setup. In light sheet microscopy, where sample illumination occurs perpendicular to detection, this 'light sheet mode' has been successfully applied to remove out-of-focus light (Baumgart and Kubitscheck, 2012). Then again, the slit can also be scanned in the propagation direction of the light sheet. Hence, by moving the focus of a Gaussian sheet with the slit, the minimum sheet thickness can be maintained over the entire FOV independent of the Rayleigh length. Until now, remote focusing of the light sheet was achieved either via a third objective lens imaging the sheet onto a mirror moved with a piezoelectric stage (Dean et al., 2015) or with a tunable acoustic gradient (TAG) lens (Zong et al., 2015; Dean and Fiolka, 2014). Piezo stages are relatively slow and/or limited in range of motion. This results in maximum frame rates of ~10 fps and a FOV typically restricted to <300 μm. Also, the required optical and mechanical elements might be difficult to include in an existing setup. TAG lenses, on the other

Received 27 April 2016; accepted in revised form 2 June 2016

REVIEW EDITOR: Prof. Alberto Diaspro

Contract grant sponsor: National Institutes of Health (NIH); Contract grant numbers: P41 GM103540 and P50 GM076516.

DOI 10.1002/iemt.22707

Published online 24 June 2016 in Wiley Online Library (wiley online library.com).

Abbreviations: ETL, electrically tunable lens; FOV, field of view; SPIM,

<sup>\*\*</sup>Robreviations: ETL, electrically unlaber lefts, FOV, field of View, STLM, selective plane illumination microscopy; TAG, tunable acoustic gradient.

\*\*Correspondence to: Enrico Gratton, Laboratory for Fluorescence Dynamics, University of California, Irvine, Biomedical Engineering Department, 3208 Natural Sciences II, Irvine, CA 92697-2715. E-mail: egratton22@gmail.com

hand, typically have to be driven with a sine wave at frequencies of >100 kHz, which is not appropriate for synchronization with a camera. This lack of synchronization again leads to a side lobe structure generating out-of-focus blur that has to be rejected by either using multi-photon excitation or a confocal detection scheme with linear deconvolution. Instead, we demonstrate here how an inexpensive electrically tunable lens (ETL) can be used to create a uniform light sheet of minimal, diffraction-limited thickness at high frame rates ( $\sim$ 40 fps) over a wide FOV (>600  $\mu$ m) without the need for multi-photon excitation or image deconvolution.

## MATERIALS AND METHODS

In most selective plane illumination microscopy (SPIM) setups, a cylindrical lens is used to generate the light sheet which is then reimaged into the sample via an objective lens. With an electrically tunable cylindrical lens, the position of the focus could be rapidly adjusted. Unfortunately, electrically tunable cylindrical lenses are currently not commercially available. Yet, a regular tunable lens combined with a few conventional optical elements can be used to achieve the desired effect. In our setup, as depicted in Figure 1a, the expanded, parallel excitation beam (488 nm, ISS, Champaign, IL) first passed a telescope consisting of two identical cylindrical lenses, CL (f = 75 mm, LJ1703RM, Thorlabs, Newton, NJ). The ETL (EL-10-30-VIS-LD, Edmund Optics, Barrington, NJ), was positioned in the center of the telescope and, hence, illuminated with a line profile. Consequently, the effective numerical aperture of the tunable lens was close to zero along the focusing, horizontal axis of the cylindrical lens pair while the full numerical aperture was utilized along the non-focusing, vertical axis. The beam exiting the telescope was parallel along the horizontal axis independent of the focal length of the tunable lens while the focal point along the vertical axis could be modulated. Since focusing of the beam into the back aperture of the excitation lens, OLE (CFI Plan Fluor 10XW, NA 0.3, Nikon, Melville, NY), flipped the light sheet axis, a forth relay lens, L (f = 75 mm, AC254-075-A, Thorlabs), was required to maintain the correct modulation axis. Fluorescence was picked up by the detection lens, OLD (XLUMPLFLN 20XW, NA 1, Olympus, Center Valley, PA), and imaged onto the chip of a sCMOS camera (Zyla 4.2, Andor, Belfast, Ireland) via a tube lens, TL (#47-740, Edmund Optics), after filtering with a long pass, F (LP500, Semrock, Rochester, NY). Whole camera chip exposure with a static light sheet is illustrated in Figure 1b. To realize the desired confocal slit detection depicted in Figure 1c, the rolling shutter of the camera was operated in 'light sheet mode' while the focus of the light sheet was modulated with the ETL. To synchronize the ETL with the virtual slit detection, a function generator (DS345, SRS, Sunnyvale, CA) generating the voltage ramp to drive the lens was triggered by the camera exposure signal, see inset in Figure 1a. A 5 ms pause between frames was introduced to allow the tunable lens to return to the initial focal position. In addition, the signal from the function generator was filtered with a home-built first order low pass with a cutoff frequency of 210 Hz to suppress oscillations of the lens (refer to datasheet for EL-10-30-VIS-LD available at www.optotune.com). These electronics as well as a voltage follower to eliminate loading effects on the function

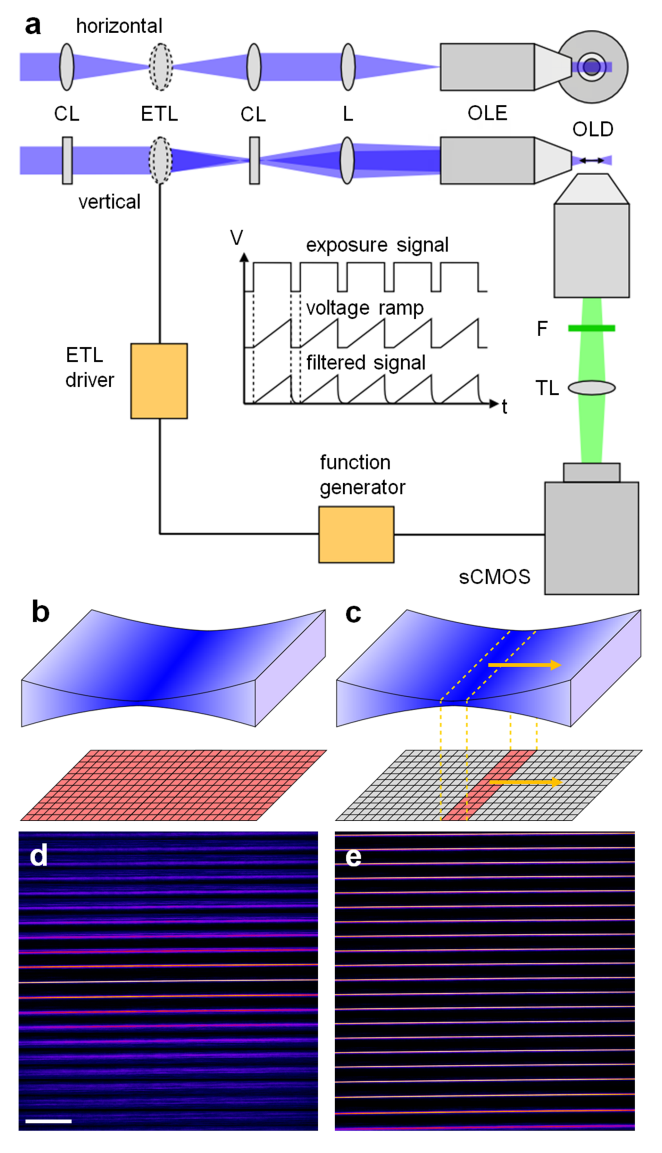


Fig. 1. (a) Schematic of the light sheet microscopy setup, refer to text for details. (b,c) Illustration of whole camera chip exposure with a static light sheet as opposed to using an axially scanned light sheet with virtual slit detection. (d,e) Montage of 21 light sheet images acquired at different y positions with a static and an axially scanned light sheet. Scale bar, 100  $\mu m$ . [Color figure can be viewed in the online issue, which is available at wileyonlinelibrary.com.]

generator were included in a home-built ETL driver. Typical ETL driving amplitudes were 0.36 V with an off-set voltage of 0.5 V. Samples were positioned and imaged as previously described (Hedde and Gratton, 2015; Hedde et al., 2015). To measure the thickness of the light sheet, we imaged the reflection off a microscope cover slip after removal of the detection filter. Figures 1d and 1e shows a montage of 21 light sheet images acquired at different y positions using a static and a modulated light sheet. Without modulation, the strong divergence of the Gaussian beam caused a rapid loss in axial resolution with increasing distance from the focus of the sheet. However, by moving the focus in sync with the virtual slit of the camera, the minimum width of the sheet could be maintained over the entire FOV.

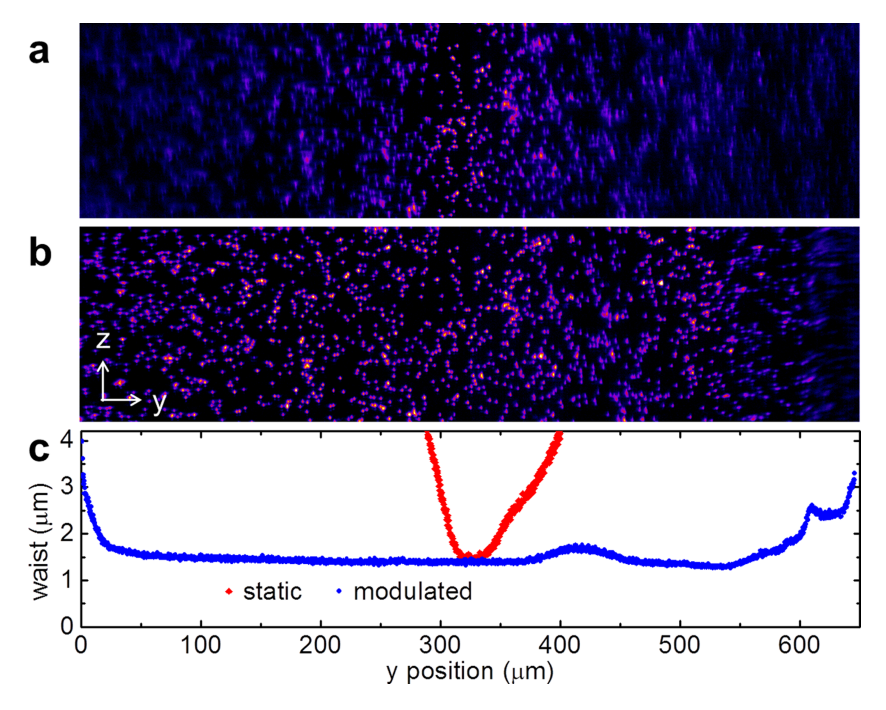


Fig. 2. Fluorescence images of 1 µm yellow-green beads embedded in a 1% agarose gel without (a) and with axial light sheet modulation (b). (c) Plot of the corresponding light sheet waist over y position without (red diamonds) and with axial light sheet modulation (blue circles). [Color figure can be viewed in the online issue, which is available at wileyonlinelibrary.com.]

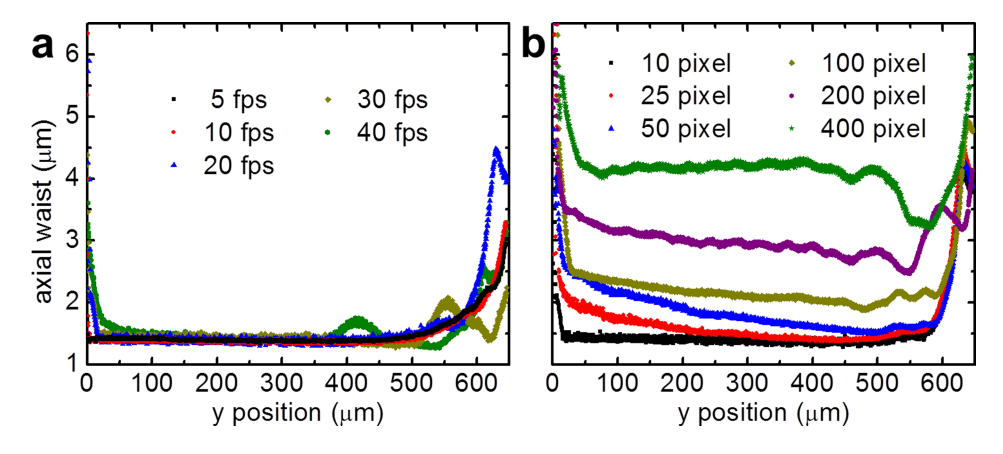


Fig. 3. Plot of the light sheet waist over y position at different frame rates (a) and different virtual slit sizes (b). One pixel, 315 nm. [Color figure can be viewed in the online issue, which is available at wileyonlinelibrary.com.]

# **RESULTS**

In order to evaluate the performance of our approach, we prepared a tissue phantom consisting of 1% low melting agarose (16520-050, Invitrogen, Carlsbad, CA) doped with 1  $\mu m$  yellow-green fluorescent microspheres (F-8823, Invitrogen) and subjected the sample to SPIM microscopy with a static as well as a modulated light sheet with synchronized virtual slit detection. Projections of the resulting image stacks along the x axis are shown in Figures 2a and 2b. The laser power was 0.28 W/cm² at the sample plane. By fluorescence excitation with a static light sheet, the

beads are clearly resolved only close to the focal point of the light sheet. The loss of axial resolution with increasing distance from the center is accompanied by increased background from out-of-focus fluorescence. By light sheet modulation with synchronized readout, the beads can be clearly resolved over more than 95% of the FOV. Only a  $\sim\!\!30~\mu\mathrm{m}$  wide disturbance is visible at the right edge of the image due to retracing of the lens. We then removed the fluorescence filter from the detection path and continuously imaged the reflection of the light sheet off a microscope cover slip while changing the distance with respect to the focal plane of

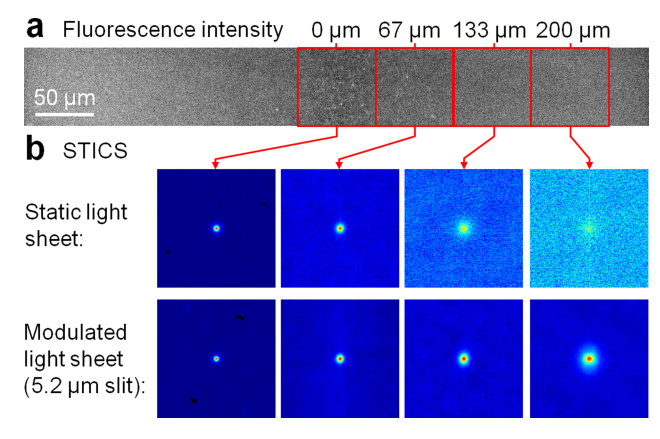


Fig. 4. STICS analysis of 20 nm beads diffusing in water solution. (a) Fluorescence intensity image of a 256 by 2,048 px<sup>2</sup> strip. (b) Spatiotemporal image correlation of 256 by 256 px<sup>2</sup> regions of interest at four different positions along the light sheet propagation axis indicated by red boxes in (a) without (top row) and with (bottom row) light sheet modulation (lag time 25 ms). [Color figure can be viewed in the online issue, which is available at wileyonlinelibrary.com.]

the detection lens. By fitting of a Gaussian to the line profiles along the y axis of those images, the width of the sheet was quantified and is plotted in Figure 2c. It can be seen that with the modulated, synchronized light sheet the waist (1/e² radius) can be maintained at 1.5  $\mu m$  over more than 90% of the FOV (650  $\mu m)$  using an excitation NA of 0.3. On the contrary, with a static, Gaussian light sheet, the v range of maximum axial resolution is limited to  $\sim 30 \mu m$  corresponding to only  $\sim$ 5% of the FOV. The data shown in Figure 2 was acquired at 40 fps and a slit width of 10 camera pixels  $(3.2 \mu m)$ . The total time per frame of 25 ms consisted of 20 ms of camera exposure followed by a 5 ms retracing pause resulting in an 80% duty cycle. The retracing pause allowed the focus of the ETL to return and settle at the initial position. The thickness of the light sheet at different frame rates is shown in Figure 3a and can be generally considered flat over >90\% of the FOV. Note that, with our camera, the minimum readout time of a full frame in 'light sheet mode' was 20 ms (50 fps), limiting the effective frame rate to 40 fps. With a faster camera, higher frame rates would be possible at the expense of a reduced duty cycle. Besides the NA of the excitation lens, the width of the virtual slit also determines the axial resolution, as plotted in Figure 3b. Besides being able to achieve high frame rates, a good axial sectioning capability is essential for the application of fluorescence fluctuation spectroscopybased approaches in thick specimen (>1 µm). As an example, we prepared a solution of 20 nm beads, the fluorescence intensity image of a 2,048 pixel long and 256 pixel wide strip along the propagation direction of the light sheet is shown in Figure 4a. An image time series of the same FOV was acquired with and without light sheet modulation with synchronized readout at a frame rate of 40 fps. The spatiotemporal image correlation was then calculated within regions of 256 by 256 pixels at increasing distances relative to the center of the FOV, as shown in Figure 4b. Without light sheet modulation, the lack of axial resolution towards the periphery of the sheet resulted in a rapid loss of the correlation amplitude. With modulation and synchronized readout, on the other hand, the correlation amplitude was much better maintained. However, it has to be said that an increase of the axial resolution by reducing the camera slit size decreases light throughput. Therefore, the slit size has to be optimized with respect to the signal available.

## DISCUSSION

In this work, we have demonstrated that an inexpensive ETL can be used to modulate the focal position of the light sheet in SPIM. Previously, this remote focusing ability has been used to improve the speed of volume imaging (Fahrbach et al., 2013; Nakai et al, 2015). Instead, we combined remote focusing via an ETL with synchronized, virtual slit detection to maintain the maximum, diffraction-limited axial resolution independently of the size of the FOV. In order to maintain a 1.5 µm width over 600 µm we used less than 10% of the available tuning range (0.36 V modulation amplitude compared to a 4 V maximum rating of the ETL). With different combinations of excitation/detection lenses this vast tuning range could be further exploited to increase resolution and/or FOV. At the same time, current sCMOS camera frame rates (~50 fps in 'light sheet mode') are supported due to the rapid response of an ETL compared to, e.g., a piezo stage (Annibale et al., 2015). Even faster lenses are available today and could handle speeds of >100 fps at a high duty cycle. Thus, this direct, deconvolution-free method is compatible with camera-based fluorescence fluctuation spectroscopy methods to probe spatiotemporal dynamics of biomolecules (Hedde et al., 2014) where the high axial resolution is crucial for the detection of the fluctuations due to single molecules. Compared to spatial light modulators or remote focusing objectives, an ETL is also easy to integrate into existing SPIM setups. Many sCMOS cameras already feature a rolling shutter that can act as a virtual slit or can be upgraded on site with new firmware.

## ACKNOWLEDGMENT

The authors thank Rachel Cinco for helpful discussion.

#### REFERENCES

Annibale P, Dvornikov A, Gratton E. 2015. Electrically tunable lens speeds up 3D orbital tracking. Biomed Opt Exp 6:2181–2190.

Baumgart E, Kubitscheck U. 2012. Scanned light sheet microscopy with confocal slit detection. Opt Exp 20:21805–21814.

Dean KM, Fiolka R. 2014. Uniform and scalable light-sheets generated by extended focusing. Opt Exp 22:26141–26152.

Dean KM, Roudot P, Welf ES, Danuser G, Fiolka R. 2015. Deconvolution-free subcellular imaging with axially swept light sheet microscopy. Biophys J 108:2807–2815.

Fahrbach FO, Rohrbach A. 2010. A line scanned light-sheet microscope with phase shaped self-reconstructing beams. Opt Exp 18: 24229–24244.

Fahrbach FO, Voigt FF, Schmid B, Helmchen F, Huisken J. 2013. Rapid 3D light-sheet microscopy with a tunable lens. Opt Exp 21: 21010–21026.

Hedde PN, Stakic M, Gratton E. 2014. Rapid measurement of molecular transport and interaction inside living cells using single plane illumination. Sci Rep 4:7048.

Hedde PN, Gratton É. 2015. Active focus stabilization for upright selective plane illumination microscopy. Opt Exp 23:14707–14714. Hedde PN, Ranjit S, Gratton E. 2015. 3D fluorescence anisotropy

Hedde PN, Ranjit S, Gratton E. 2015. 3D fluorescence anisotropy imaging using selective plane illumination microscopy. Opt Exp 23: 22308–22317.

Huisken J, Swoger J, Del Bene F, Wittbrodt J, Stelzer EHK. 2004. Optical sectioning deep inside live embryos by selective plane illumination microscopy. Science 13:1007–1009.

- Nakai Y, Ozeki M, Hiraiwa T, Tanimoto R, Funahashi A, Hiroi N, Taniguchi A, Nonaka S, Boilot V, Shrestha R, Clark J, Tamura N, Draviam VM, Oku H. 2015. High-speed microscopy with an electrically tunable lens to image the dynamics of in vivo molecular complexes. Rev Sci Instrum 86:013707.
- Planchon TA, Gao L, Milkie DE, Davidson MW, Galbraith JA, Galbraith CG, Betzig E. 2011. Rapid three-dimensional isotropic imaging of living cells using Bessel beam plane illumination. Nat Methods 8:417–423.
- Vettenburg T, Dalgarno HIC, Nylk J, Coll-Lladó C, Ferrier DEK, Čižmár T, Gunn-Moore FJ, Dholakia K. 2014. Light-sheet microscopy using an Airy beam. Nat Methods 11:541–544.
- Voie H, Burns DH, Spelman FA. 1993. Orthogonal-plane fluorescence optical sectioning: Three dimensional imaging of macroscopic biological specimens. J Microsc 170:229–236.

  Zong W, Zhao J, Chen X, Lin Y, Ren H, Zhang Y, Fan M, Zhou Z, Cheng
- Zong W, Zhao J, Chen X, Lin Y, Ren H, Zhang Y, Fan M, Zhou Z, Cheng H, Sun Y, Chen L. 2015. Large-field high-resolution two-photon digital scanned light-sheet microscopy. Cell Res 25:254–257.

Copyright of Microscopy Research & Technique is the property of John Wiley & Sons, Inc. and its content may not be copied or emailed to multiple sites or posted to a listserv without the copyright holder's express written permission. However, users may print, download, or email articles for individual use.